Proceedings of the ASME 2010 3rd Joint US-European Fluids Engineering Summer Meeting and 8th International Conference on Nanochannels, Microchannels, and Minichannels
FEDSM-ICNMM2010
August 1-5, 2010, Montreal, Canada

FEDSM-ICNMM2010-30384

AEROTHERMOELASTIC STABILITY OF FUNCTIONALLY GRADED CIRCULAR CYLINDRICAL SHELLS

Farhad Sabri
Department of Mechanical Engineering, Ecole Polytechnique de Montreal
Montreal, Canada
farhad.sabri@polymtl.ca

Aouni. A. Lakis
Department of Mechanical Engineering, Ecole Polytechnique de Montreal
Montreal, Canada
aouni.lakis@polymtl.ca

ABSTRACT

In this work, a hybrid finite element formulation is presented to predict the flutter boundaries of circular cylindrical shells made of functionally graded materials. The development is based on the combination of linear Sanders thin shell theory and classic finite element method. Material properties are temperature dependent, and graded in the shell thickness direction according to a simple power law distribution in terms of volume fractions of constituents. The temperature field is assumed to be uniform over the shell surface and along the shell thickness. First order piston theory is applied to account for supersonic aerodynamic pressure. The effects of temperature rise and shell internal pressure on the flutter boundaries of FG circular cylindrical shell for different values of power law index are investigated. The present study shows efficient and reliable results that can be applied to the aeroelastic design and analysis of shells of revolution in aerospace vehicles.

INTRODUCTION

Increasing need to manufacture light-weight aerospace structure has resulted in the production of new advanced materials like new composite materials. Consequently, application of functionally graded materials (FGM) in the advanced aircraft structures has attracted wide attention recently among the aerospace engineers. Since the skin of aerospace vehicles are made of cylindrical shell and experience high temperature field, the use of FGMs as their protection materials can be efficient. Therefore, an appropriate design and analysis method for analysis of such structures is needed.

A comprehensive description about the FGMs properties and their applications can be found in Refs. [1] [2]. Recently, vibration and dynamic analysis of shell and plates made of FGMs subjected to high temperature environmental has received attention among the researches [3-8]. Those investigations are conducted either analytically or numerically on the prediction of dynamic (vibration) and static (buckling) stabilities of the structure due to different thermal and mechanical loadings. Material properties are graded mostly based on the simple power law distribution in terms of volume fraction of constituents. But aerothermoelastic analysis of shell and plates made of FGMs has been investigated by a few studies. Prakash et al [9], Navazi et al [10] and Hesham et al [11] works predicts the flutter of FG plates. Haddadpour et al [12] investigated the post-flutter prediction of FG plate. Aeroelastic analysis of FG circular cylindrical shells has been addressed in Ref. [13] and for a truncated conical shell in Ref. [14]. Those mentioned aeroelastic studies although provides a good prediction for supersonic flutter speed but for such a problem which contains complex structures, boundary conditions, material and loadings, an analytical model becomes very complicated and it is not sufficiently a powerful method to contain all the features affecting flutter boundaries. Also they are computationally expensive, which is not desired during the preliminary design of a modern aircraft structures. Therefore the objective of this study is to propose an efficient FEM to adequately describe supersonic flutter of a FG cylindrical shell at less computational cost and effort. The linear Sanders thin shell theory is combined with classic finite element method to derive the exact solution for shape functions rather than approximation by polynomial functions. This method leads to a very fast and precise convergence where it was applied by the same authors [15], for flutter prediction of isotropic cylindrical shells subjected to supersonic flow.

STRUCTURAL MODELING

Strain vector in terms of displacement fields, axial U, radial W and circumferential V directions; based on the linear Sanders thin shell theory is written in cylindrical coordinate system as [16]:

$$\begin{Bmatrix} \varepsilon_x \\ \varepsilon_\theta \\ \varepsilon_{x\theta} \\ \kappa_x \\ \kappa_\theta \\ \kappa_{x\theta} \end{Bmatrix} = \begin{Bmatrix} \dfrac{\partial U}{\partial x} \\ \dfrac{1}{R}\dfrac{\partial V}{\partial \theta}+\dfrac{W}{R} \\ \dfrac{1}{2}(\dfrac{\partial V}{\partial x}+\dfrac{1}{R}\dfrac{\partial U}{\partial \theta}) \\ -\dfrac{\partial^2 W}{\partial x^2} \\ -\dfrac{1}{R^2}\dfrac{\partial^2 W}{\partial \theta^2}+\dfrac{1}{R^2}\dfrac{\partial V}{\partial \theta} \\ -\dfrac{1}{R}\dfrac{\partial^2 W}{\partial \theta \partial x}+\dfrac{3}{4R}\dfrac{\partial V}{\partial x}-\dfrac{1}{4R^2}\dfrac{\partial U}{\partial \theta} \end{Bmatrix} \tag{1}$$

where ε_x, ε_θ, $\varepsilon_{x\theta}$ are the normal strain referred to mid-surface and κ_x, κ_θ, $\kappa_{x\theta}$ are the change in curvature of mid-surface normal.

CONSTITUTIVE RELATION

Functionally graded materials (FGM) are made from the combination of different material with different volume fraction of their constituents. Their material properties could be temperature dependent and are graded in the shell thickness. In this work, the material properties P are considered temperature dependent as [1]:

$$P = P_0\left(P_{-1}T^{-1}+1+P_1T+P_2T^2+P_3T^3\right) \tag{2}$$

where T is working temperature in Kelvin and P_{-1}, P_2 and P_3 are constant coefficients with different values for different materials. Also it is assumed that the shell is made from the mixture of a ceramic as high-resistant material against high temperature loading and a metal as an element to support mechanical loadings. Material properties are graded along thickness of shell where the effective one is defined as:

$$P_e(z) = P_cV_c + P_mV_m \tag{3}$$

P_c and P_m are material properties of ceramic and metal respectively with their corresponding volume fractions V_c and V_m. It is assumed that the outer skin of the shell is ceramic rich and the inner side is metal rich; therefore, the volume fractions based on the simple power law distribution are found as:

$$V_c = (0.5+\frac{z}{h})^N \tag{4}$$

$$V_m = 1 - V_c \tag{5}$$

where h is the shell thickness and N is the volume fraction exponents. Upon selection of different values for N, variation of material properties along the shell thickness are reported in the Fig. 1.

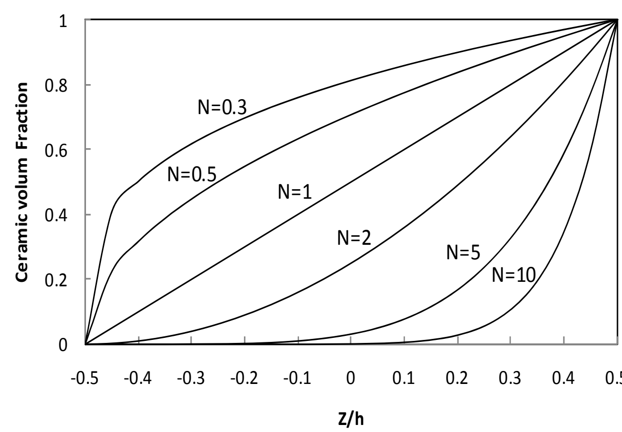

Fig. 1 Variation of ceramic volume fraction

The constitutive relation for non zero strains are given by:

$$\{\sigma\} = [P]\{\varepsilon\} \tag{6}$$

In above relation *[P]* is the reduced stuffiness matrix and defined as:

$$[P] = \begin{bmatrix} D & \upsilon D & 0 & 0 & 0 & 0 \\ \upsilon D & D & 0 & 0 & 0 & 0 \\ 0 & 0 & \dfrac{D(1-\upsilon)}{2} & 0 & 0 & 0 \\ 0 & 0 & 0 & K & \upsilon K & 0 \\ 0 & 0 & 0 & \upsilon K & K & 0 \\ 0 & 0 & 0 & 0 & 0 & \dfrac{K(1-\upsilon)}{2} \end{bmatrix} \tag{7}$$

where

$$K = \frac{E(z)h^3}{12(1-\upsilon^2(z))}$$
$$D = \frac{E(z)h}{1-\upsilon^2(z)} \tag{8}$$

In the above relations, $E(z)$ is module of elasticity and $\nu(z)$ is the Poisson's ratio for assumed FG cylinder. Carrying the integration of Eq. (6) along the shell thickness results the normal stress and moment resultants and by replacing them in the Sanders equations of equilibrium, following implicit relations in terms of displacements components and their derivatives are obtained:

$$\begin{aligned} &L_1(U,W,V,Q_{ij}) = 0 \\ &L_2(U,W,V,Q_{ij}) = 0 \\ &L_3(U,W,V,Q_{ij}) = 0 \end{aligned} \tag{9}$$

Details of above equations are reported in Appendix. Considering the displacements as period functions, they can be expressed in Fourier series as:

$$\begin{aligned} U(x,\theta) &= \sum_{n=0}^{\infty} u_n(x)\cos(n\theta) \\ W(x,\theta) &= \sum_{n=0}^{\infty} w_n(x)\cos(n\theta) \\ V(x,\theta) &= \sum_{n=0}^{\infty} v_n(x)\sin(n\theta) \end{aligned} \tag{10}$$

Upon substitution of these functions in the Eq. (9), with the help of solution for roots of obtained characteristic equation, the final form of displacements can be found as [15]:

$$\begin{Bmatrix} U(x,\theta) \\ W(x,\theta) \\ V(x,\theta) \end{Bmatrix} = [T][R]\{C_i\} \tag{11}$$

where the matrices *[T]* and *[R]* are defined in Appendix. Relation (11) states the exact solution of displacements obtained from the Sanders thin shell theory.

FRUSTUM ELEMENT

Cylindrical shell is discretized by finite frustum elements (see fig. 2). Each finite element has two nodal lines with four degrees of freedom. Because of type of elements, the shape functions estimating the elements deformation along its lengths between two nodal lines, are found from exact solution of shell theory. Consequently it leads to the very fast and precise convergence compared to the traditional finite element method where the shape functions are approximated by polynomial functions.

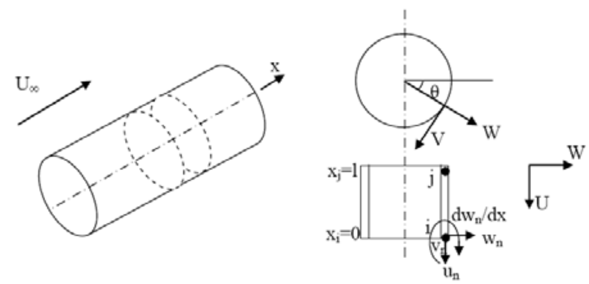

Fig. 2 Shell element geometry

The accuracy of this method has been established well in Ref. [15]. Assuming the nodal degrees of freedom vector in terms of element displacement vector, it is expressed as:

$$\begin{Bmatrix} \delta_i \\ \delta_j \end{Bmatrix} = \{u_{ni}, w_{ni}, \partial w_{ni}/\partial x, v_{ni}, u_{nj}, w_{nj}, \partial w_{nj}/\partial x, v_{nj}\}^T = [A]\{C_i\} \tag{12}$$

where the components of matrix $[A]$ is found from the element of $[R]$ (see Appendix). Therefore, displacement vectors (Eq. (11)) with the help of Eq. (12) is rewritten as:

$$\begin{Bmatrix} U(x,\theta) \\ W(x,\theta) \\ V(x,\theta) \end{Bmatrix} = [T][R][A]^{-1}\begin{Bmatrix} \delta_i \\ \delta_j \end{Bmatrix} = [N]\begin{Bmatrix} \delta_i \\ \delta_j \end{Bmatrix} \tag{13}$$

where $[N]$ matrix is corresponding to the shape function of this proposed hybrid analytical-finite element method.

STRUCTURE MASS AND STIFFNESS MATRIX

Strain vector can be expressed in terms of nodal degree of freedom with the help of eq. (13) as:

$$\{\varepsilon\} = \begin{bmatrix} [T] & [0] \\ [0] & [T] \end{bmatrix}[Q][A^{-1}]\begin{Bmatrix} \delta_i \\ \delta_j \end{Bmatrix} = [B]\begin{Bmatrix} \delta_i \\ \delta_j \end{Bmatrix} \tag{14}$$

where matrix $[Q]$ is reported in Appendix. Following the standard procedure in finite element method structure stiffness matrix $[k]$ and structure mass matrix $[m]$ are found as:

$$[k_s] = \int_0^l \int_0^{2\pi} [B]^T [P][B] r dx d\theta \tag{15}$$

$$[m_s] = \rho_e h \int_0^l \int_0^{2\pi} [N]^T [N] r dx d\theta \tag{16}$$

where

$$\rho_e = \int_{-h/2}^{h/2} \rho(z)dz \tag{17}$$

The pre-buckling membrane stress resultants corresponding to pressure differential across the shell P_m, axial compression P_x and temperature difference ΔT, represented by the components of the following diagonal matrix:

$$\left[N_0\right]=\begin{bmatrix} N_x & 0 & 0 \\ 0 & N_\theta & 0 \\ 0 & 0 & N_x+N_\theta \end{bmatrix} \tag{18}$$

where

$$N_x = -\frac{P_x}{2\pi R} - \int_{-h/2}^{h/2} \frac{E(z)\alpha(z)}{1-\upsilon(z)} \Delta T(z)dz \tag{18}$$

$$\overline{N}_\theta = P_m R \tag{19}$$

where α is the thermal expansion of the shell. The geometric stiffness matrix of a shell element can be found from the expression for the potential energy due to this initial strain:

$$U_i = \frac{1}{2}\int_0^l \int_0^{2\pi} \{\beta\}^T \left[N_0\right]\{\beta\} rdxd\theta \tag{20}$$

where $\{\beta\}$ is the elastic rotation vector based on Sanders thin shell theory [16]:

$$\{\beta\} = \begin{Bmatrix} -\dfrac{\partial W}{\partial x} \\ \dfrac{1}{R}(V - \dfrac{\partial W}{\partial \theta}) \\ \dfrac{1}{2}(-\dfrac{1}{R}\dfrac{\partial U}{\partial \theta} + \dfrac{\partial V}{\partial x}) \end{Bmatrix} \tag{21}$$

Upon substitution of displacement fields based on the shape function in the above equation and then replacing back in the Eq. (2), element geometric stiffness matrix is found as:

$$[k_G] = \int_0^l \int_0^{2\pi} [N]^T [C_0]^T \begin{bmatrix} N_x & 0 & 0 \\ 0 & N_\theta & 0 \\ 0 & 0 & N_x+N_\theta \end{bmatrix} [C_0]^T [N]^T \, Rd\theta dx \tag{22}$$

where $\left[C_0\right]$ is the derivative matrix of shape functions comprised from inserting the displacement fields in Eq. (21). This stiffness matrix is added to the one developed in Eq. (15).

AERODYNAMIC MODELING

In this study aerodynamic pressure loading due to supersonic airflow is modeled based on the first order piston theory where it is expressed as:

$$P_a = \frac{\gamma p_\infty M^2}{(M^2-1)^{1/2}} \left[\frac{\partial W}{\partial x} + \frac{M^2-2}{M^2-1}\frac{1}{U_\infty}\frac{\partial W}{\partial t} - \frac{W}{2R(M^2-1)^{1/2}} \right] \tag{23}$$

where p_∞, U_∞, M and γ are the freestream static pressure, freestream velocity, Mach number and adiabatic expansion of air, respectively. With the help of shape function relation for radial deflection (Eq. (13)), this pressure field in terms of nodal degree of freedom is written as:

$$\begin{aligned} \{P_a\} = \begin{Bmatrix} 0 \\ p_{radial} \\ 0 \end{Bmatrix} &= \frac{-\rho_\infty U_\infty^2}{(M^2-1)^{1/2}} \frac{1}{U_\infty} (\frac{M^2-2}{M^2-1})[T][R_f][A^{-1}] \begin{Bmatrix} \dot{\delta}_i \\ \dot{\delta}_j \end{Bmatrix} \\ &+ (i\frac{\lambda_j}{R}) \frac{-\rho_\infty U_\infty^2}{(M^2-1)^{1/2}} [T][R_f][A^{-1}] \begin{Bmatrix} \delta_i \\ \delta_j \end{Bmatrix} \\ &- \frac{-\rho_\infty U_\infty^2}{(M^2-1)^{1/2}} (\frac{1}{2(M^2-1)^{1/2} R})[T][R_f][A^{-1}] \begin{Bmatrix} \delta_i \\ \delta_j \end{Bmatrix} \end{aligned} \tag{24}$$

where the first term results in aerodynamic damping matrix and the second and third terms result in aerodynamic stiffness matrix.

AEROELASTIC MODEL

The final form of governing equation in global system for a FG cylindrical shell subjected to a supersonic flow and under pre-stress con**d**ition due to mechanical and thermal loading will be:

$$\left[M_S\right]\{\ddot{\delta}\} - \left[C_a\right]\{\dot{\delta}\} + \left(\left[K_S\right] + \left[K_G\right] - \left[K_a\right]\right)\{\delta\} = 0 \tag{25}$$

where subscripts S, a and G refer to structure, aerodynamic loading and geometric stiffness due to initial membrane forces; respectively. Aeroelastic stability of the shell is investigated by studying the eigenvalue of Eq. (25) in the complex plane. Flutter onset occurs when the imaginary part of the eigenvalue changes from positive to negative value. That imaginary part represents the damping of the system while the real part shows the oscillation frequency.

RESULT AND DISCUSSION

In this study considered cylindrical shell is made of ceramic, Silicon Nitride (Si_3N_4), at the outer surface and stainless still (SUS304) on the inner surface. Their material properties can be found in the Table1. The characteristics of airflow is considered as: $M = 3$, $a_\infty = 213 \ m/s$, $T_{t\infty} = 49^\circ C$.

Table1. Material properties of FGM, Ref. [1]

Material	P_0	P_{-1}	P_1	P_2	P_3
Silicon nitride					
E (pa)	348.43E9	0	-3.07E-4	2.160E-7	-8.946E-11
α (/K)	5.8723E-6	0	9.095E-4	0	0
Y	0.2400	0	0	0	0
ρ (kg/m^3)	2370	0	0	0	0
Stainless – Steel					
E (pa)	201.04e9	0	3.079e-4	2.160e-7	-8.946e-11
α (/K)	12.33e-6	0	8.086e-4	0	0
Y	0.3262	0	-2.002e-4	0	0
ρ (kg/m^3)	8166	0	0	0	0

A convergence test for a simply supported FG cylindrical shell with different gradual variation of material properties has been reported in Tables 2. It shows a very fast convergence with only 12 elements therefore, using 20 elements will be sufficient to obtain reliable results for further analysis.

Tale 2 Convergence test for critical flutter onset

	Ceramic rich, *N=0*	*N=3*	*N=20*
No. Elements	P_∞ (KPa)	P_∞ (KPa)	P_∞ (KPa)
5	20.86	0.38	0.13
8	29.79	7.60	5.67
10	31.12	8.89	6.66
12	31.72	9.48	7.13
15	32.14	9.95	7.47
18	32.35	10.12	7.67
20	32.43	10.21	7.71

In order to see the effect of material volume fraction N , on the aeroelastic stability prediction, for a ceramic reach $N=0$ shell and $N=3$, real and imaginary parts of eigenvalue versus freestream static pressure have been plotted in Figs. 3 and 4, by increasing the static pressure, real parts of first and second axial mode converge to each other, and eventually they merge together, representing the oscillation frequency. When we have crossed zero for one of the imaginary parts of eigenvalues representing the damping of the system, flutter onset happens. It occurs for $N=0$ at $P_\infty = 33000Pa$ and for $N=3$ at $P_\infty = 10000Pa$.

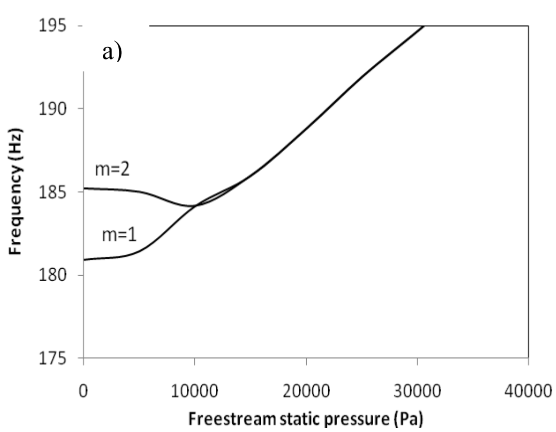

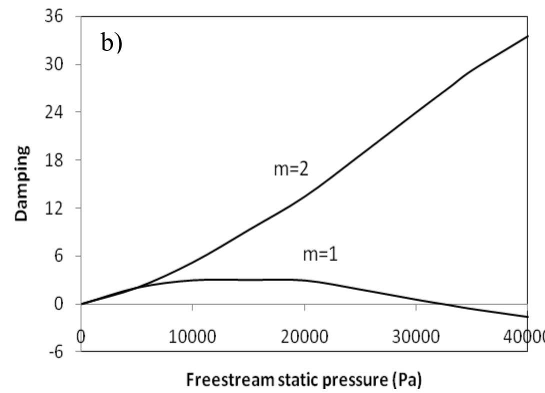

Fig.3 a) Real part b) imaginary part of eigenvalue versus freesteram static pressure, n=25; ceramic rich N=0

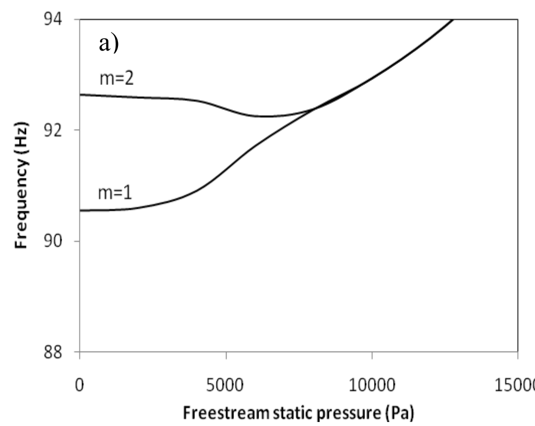

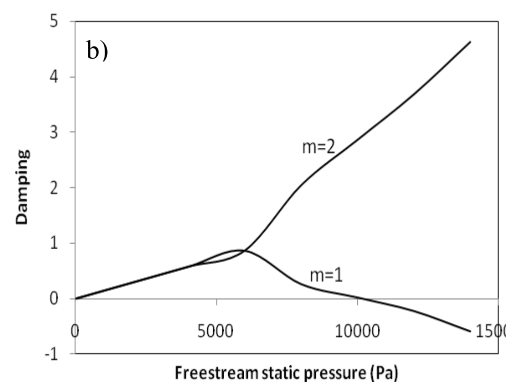

Fig.4 a) Real part; b) imaginary part of eigenvalue versus freesteram static pressure, n=25; N=3

It can be seen that, for *N=0*, shell losses its stability at higher freestream static pressure compared to the case of *N=3*. This critical flutter onset for different values of N and internal pressure has been reported in Fig. 5. It shows that for smaller N , shell has more flutter resistant, since the material properties are close to ceramic *(N=0)*. Also for pressurized shell, flutter instability occurs at higher freestream static pressure.

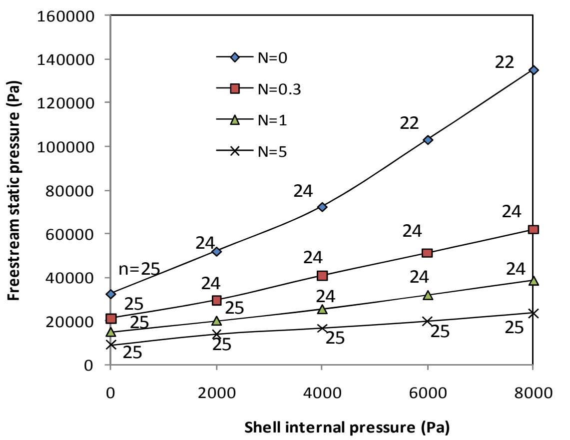

Fig. 5 Flutter boundaries for pressurized FG cylindrical shell

In Table 3 the effect of temperature rise on flutter boundaries has been reported for free internal pressure shell. It is assumed that temperature is under the critical buckling temperature and it has uniform distribution along the shell length and thickness where it has reached that initial final temperature. The free stress temperature for shell is 300 K. It can be seen that how temperature raise will decrease the critical flutter freestream static pressure.

Table 3 Effect of Temperature on flutter boundaries

	ΔT=50	ΔT=100	ΔT=150
N	P_∞(Pa)	P_∞(Pa)	P_∞(Pa)
0	22800	6870	4440
0.3	17500	1880	1330
1	13900	1120	920
3	4700	530	230

CONCLUSION

An efficient hybrid analytical-finite element method has been developed for aerothermoelastic instability prediction of cylindrical shell made of functionally graded materials. This linear method will be useful to detect the bifurcation points for further nonlinear analysis of stability threshold. Due to smaller value of power index for ceramic volume fraction shell shows more flutter resistant while for larger values, shell losses its stability at higher velocities through coupled mode flutter. Since the shell becomes stiffer by increasing the internal pressure, the flutter velocity is predicted at higher value for pressurized FG shell. Increasing temperature will affect the stability of the shell where the flutter onset happens at lower velocities. This proposed method can provide efficient and reliable results at less computation time and efforts compared to the other analytical and commercial FEM and can be applied with high fidelity for aerothermoelastic analysis of aerospace structures.

REFERENCES

[1] J.N. Reddy and C.D. Chin, "Thermomechanical Analysis of Functionally Graded Cylinders and Plates", Journal of Thermal Stress,1998; 21: 593-626.
[2] S. Suresh and A. Mortensen, "Fundamentals of Functionally Graded Materials: Processing and Thermo-Mechanical Behavior of Graded Metals and Metal Ceramic Composites, IOM Communications, London, 1998.
[3] H. Haddadpour, S. Mahmoudkhani and H.M. Navazi, " Free Vibration Analysis of Functionally Graded Cylindrical Shells Including Thermal Effects", Journal of Thin Walled Structures, 2007;45:591-599.
[4] R. Kadoli, N. Ganesan, "Buckling and Free Vibration Analysis of Functionally Graded Cylindrical Shells Subjected to a Temperature-Specified Boundary Condition", Journal of Sound and Vibration, 2006;298:450-480.
[5] S.C. Pradhan, C.T. Loy, K.Y. Lam and J.N. Reddy," Vibration characteristics of Functionally Graded Cylindrical Shells Under Various Boundary Condition", Applied Acoustics, 2006;61:111-129.
[6] L. Wu, Z. Jiang and J. Liu," Thermoelastic Stability of Functionally Graded Cylindrical Shells", Journal of Thermal Stresss, 2005;70:60-68.
[7] H.-S. Shen and N. Noda, "Postbuckling of FGM Cylindrical Shells Under Combined Axial and radial Mechanical Loads in Thermal Environments", International Journal of Solids Structures, 2005;42:4641-4662.
[8] B. Mirzavand and M. R. Eslami, "Thermal Buckling of Imperfection Functionally Graded Cylindrical Shells Based On The Wan-Donnel Model", Journal of Thermal Stresses, 2006;29:37-55.
[9] T. Prakash and M. Ganapathi, " Supersonic Flutter Characteristics of Functionally Graded Panels Including Thermal Effects", Journal of Composites Structures, 2006; 72:10-18.
[10] H. M. Navazi and H. Haddadpour, " Aero-thermoelastic Stability of Functionally Graded Plates", Journal of Composite Structures, 2007;80:580-587.
[11] H. H. Ibrahim, H. H. Yoo and K.-S. Lee, "Supersonic Flutter of Functionally Graded Panels Subjected to Acoustic an Thermal Loads", Journal of Aircrfat. 2009; 46(2):593-600.
[12] H. Haddadpour, H.M. Navazi and F. Shadmehri, "Nonlinear Oscillation of A Fluttering Functionally Graded Plate", Journal of Composite Structures,2007;79:242-250.
[13] H. Haddadpour, S. Mahmoudkhani and H. M. Navazi, "Supersonic Flutter Prediction of Functionally Graded Cylindrical Shells" Journal of Composites Structures, 2008;83: 391-398.
[14] S. Mahmoudkhani, H. Haddadpour and H. M. Navazi, "Supersonic Flutter Prediction of Functionally Graded Conical Shell" Journal of Composite Structures, 2010;92:377-386.
[15] F. Sabri, and A. A. Lakis "Finite Element Method Applied to Supersonic Flutter of Circular Cylindrical Shells," AIAA Journal,2010;48:73-81.

[16] J. L. Sanders, "An Improved First-Approximation Theory for Thin Shell," NASA R-24. 1959.

APPENDIX

I. Sanders equations of equilibrium in terms of displacement components and their derivatives are (Eq. (9)):

$$L_1(U,V,W,P_{ij}) = P_{11}\frac{\partial^2 U}{\partial x^2} + \frac{P_{12}}{R}\frac{\partial^2 U}{\partial x^2}(\frac{\partial^2 V}{\partial x\partial\theta} + \frac{\partial W}{\partial x}) - P_{14}\frac{\partial^3 W}{\partial x^3}$$
$$+\frac{P_{15}}{R^2}(\frac{\partial^3 W}{\partial x\partial\theta^2} + \frac{\partial^2 V}{\partial x\partial\theta}) + (\frac{P_{33}}{R} - \frac{P_{63}}{2R^2})(\frac{\partial^2 V}{\partial x\partial\theta} + \frac{1}{R}\frac{\partial^2 U}{\partial\theta^2})$$
$$+(\frac{P_{36}}{R^2} - \frac{P_{66}}{2R^3})(-2\frac{\partial^3 W}{\partial x\partial\theta^2} + \frac{3}{2}\frac{\partial^2 V}{\partial x\partial\theta} - \frac{1}{2R}\frac{\partial^2 U}{\partial\theta^2})$$

$$L_2(U,V,W,P_{ij}) = (\frac{P_{21}}{R} - \frac{P_{51}}{R^2})\frac{\partial^2 U}{\partial x\partial\theta} + \frac{1}{R}(\frac{P_{22}}{R} + \frac{P_{52}}{R^2})(\frac{\partial^2 V}{\partial\theta^2} + \frac{\partial W}{\partial\theta})$$
$$-(\frac{P_{24}}{R} + \frac{P_{54}}{R^2})\frac{\partial^3 W}{\partial x^2\partial\theta} + \frac{1}{R^2}(\frac{P_{25}}{R} + \frac{P_{55}}{R^2})(-\frac{\partial^3 W}{\partial\theta^3} + \frac{\partial^2 V}{\partial\theta^2})$$
$$+(P_{33} + \frac{3P_{63}}{2R})(\frac{\partial^2 V}{\partial x^2} + \frac{\partial^2 U}{R\partial x\partial\theta})$$
$$+\frac{1}{R}(P_{36} + \frac{3P_{66}}{2R})(-2\frac{\partial^3 W}{\partial x^2\partial\theta} + \frac{3}{2}\frac{\partial^2 V}{\partial x^2} - \frac{1}{2R}\frac{\partial^2 U}{\partial x\partial\theta})$$

$$L_3(U,V,W,P_{ij}) = P_{41}\frac{\partial^3 U}{\partial x^3} + \frac{P_{42}}{R}(\frac{\partial^3 V}{\partial x^2\partial\theta} + \frac{\partial^2 W}{\partial x^2}) - P_{44}\frac{\partial^4 W}{\partial x^4}$$
$$+\frac{P_{45}}{R^2}(-\frac{\partial^4 W}{\partial x^2\partial\theta^2} + \frac{\partial^3 V}{\partial x^2\partial\theta}) + \frac{2P_{63}}{R}(\frac{1}{R}\frac{\partial^3 U}{\partial x\partial\theta^2} + \frac{\partial^3 V}{\partial x^2\partial\theta})$$
$$+\frac{2P_{66}}{R^2}(-2\frac{\partial^4 W}{\partial x^2\partial\theta^2} + \frac{3}{2}\frac{\partial^3 V}{\partial x^2\partial\theta} - \frac{1}{2R}\frac{\partial^3 U}{\partial x\partial\theta^2}) + \frac{P_{51}}{R^2}\frac{\partial^3 U}{\partial x\partial\theta^2}$$
$$+\frac{P_{52}}{R^3}(\frac{\partial^3 V}{\partial\theta^3} + \frac{\partial^2 W}{\partial\theta^2}) + \frac{P_{55}}{R^4}(-\frac{\partial^4 W}{\partial\theta^4} + \frac{\partial^3 V}{\partial\theta^3}) - \frac{P_{21}}{R}\frac{\partial U}{\partial x} - \frac{P_{54}}{R^2}\frac{\partial^4 W}{\partial x^2\partial\theta^2}$$
$$+\frac{P_{22}}{R^2}(\frac{\partial V}{\partial\theta} + W) + \frac{P_{24}}{R^2}\frac{\partial^2 W}{\partial\theta^2} - \frac{P_{25}}{R^3}(-\frac{\partial^2 W}{\partial\theta^2} + \frac{\partial V}{\partial\theta})$$

where P_{ij} are the component of reduced stiffness matrix defined in Eq. (7).

II. Matrices $[T]_{3\times3}$, $[R]_{3\times8}$, $[A]_{8\times8}$ and $[Q]_{6\times8}$ are defined as:

$$[T] = \begin{bmatrix} \cos(n\theta) & 0 & 0 \\ 0 & \cos(n\theta) & 0 \\ 0 & 0 & \sin(n\theta) \end{bmatrix}$$

$$R(1,i) = \alpha_i e^{\lambda_i x/R} \quad , \quad R(2,i) = e^{\lambda_i x/R}$$
$$, \quad R(1,i) = \beta_i e^{\lambda_i x/R} \qquad i = 1,2,...,8$$

$$A(1,i) = \alpha_i, \quad A(2,i) = 1, \quad A(3,i) = \frac{\lambda_i}{R},$$
$$A(4,i) = \beta_i, \quad A(5,i) = \alpha_i e^{\lambda_i l/R}$$
$$A(6,i) = e^{\lambda_i l/R}, \quad A(7,i) = \frac{\lambda_i}{R}e^{\lambda_i l/R},$$
$$A(8,i) = \beta_i e^{\lambda_i l/R} \qquad i = 1,2,...8$$

$$Q(1,i) = \alpha_i\frac{\lambda_i}{R}e^{\lambda_i x/R}, \quad Q(2,i) = \frac{1}{R}(n\beta_i + 1)e^{\lambda_i x/R},$$
$$Q(3,i) = \frac{1}{R}(\beta_i\lambda_i - n\alpha_i)e^{\lambda_i x/R} \quad Q(4,i) = -(\frac{\lambda_i}{R})^2 e^{\lambda_i x/R},$$
$$Q(5,i) = \frac{1}{R^2}(n^2 + \beta_i n)e^{\lambda_i x/R},$$
$$Q(6,i) = \frac{1}{R^2}(2n\lambda_i + \frac{3}{2}\beta_i\lambda_i + \frac{1}{2}n\alpha_i)e^{\lambda_i x/R}$$
$$i = 1,2,...8$$